European Journal of Cell Biology 99 (2020) 151059

Contents lists available at ScienceDirect

European Journal of Cell Biology

journal homepage: www.elsevier.com/locate/ejcb

Research paper

# Proteomic and cell biological profiling of the renal phenotype of the *mdx-4cv* mouse model of Duchenne muscular dystrophy

Paul Dowling[a,b], Margit Zweyer[c], Maren Raucamp[c], Michael Henry[d], Paula Meleady[d], Dieter Swandulla[c], Kay Ohlendieck[a,b,*]

[a] Department of Biology, Maynooth University, National University of Ireland, Maynooth W23F2H6, Co. Kildare, Ireland
[b] Kathleen Lonsdale Institute for Human Health Research, Maynooth University, Maynooth W23F2H6, Co. Kildare, Ireland
[c] Institute of Physiology II, University of Bonn, D53115 Bonn, Germany
[d] National Institute for Cellular Biotechnology, Dublin City University, Dublin 9, Ireland

ARTICLE INFO

*Keywords:*
Dystrophin
Dystrophinopathy
Ectopic fat
FABP1
Fatty acid binding protein
Kidney disease

ABSTRACT

The X-linked inherited muscle wasting disease Duchenne muscular dystrophy, which is caused by primary abnormalities in the membrane cytoskeletal protein dystrophin, is a multi-system disorder. Highly progressive forms of dystrophinopathy are associated with a complex secondary pathophysiology, including renal dysfunction. It was therefore of interest to carry out a systematic survey of potential proteome-wide changes in the kidney of the established *mdx-4cv* mouse model of dystrophinopathy. Of 5878 mass spectrometrically identified kidney proteins, 82 versus 142 proteins were shown to be decreased or increased, respectively, in association with muscular dystrophy. The most decreased versus increased protein species are the ACSM3 isoform of mitochondrial acyl-coenzyme A synthetase and the FABP1 isoform of fatty acid binding protein, respectively. Both proteomic findings were verified by immunofluorescence microscopy and immunoblot analysis. Interestingly, haematoxylin/eosin staining indicated diffuse whitish deposits in the *mdx-4cv* kidney, and an increased intensity of Sudan Black labelling of kidney cells revealed ectopic fat deposition. Although the proteomic results and cell biological findings do not demonstrate a direct functional link between increased FABP1 and fat accumulation, the results suggest that the up-regulation of FABP1 may be related to abnormal fat metabolism. This makes FABP1 potentially a novel pathobiochemical indicator for studying kidney abnormalities in the *mdx-4cv* model of dystrophinopathy.

## 1. Introduction

Paediatric neuromuscular disorders include a variety of mostly inherited diseases of the peripheral nervous system and the skeletal musculature, including several types of muscular dystrophy (Dowling et al., 2018). X-linked Duchenne muscular dystrophy is characterized by primary abnormalities in the *DMD* gene (Koenig et al., 1987; Guiraud et al., 2015), which encodes the membrane cytoskeletal protein dystrophin that belongs to the spectrin-like superfamily of actin-crosslinking proteins (Koenig et al., 1988; Delalande et al., 2017). A range of genetic mutations results in the almost complete loss of the full-length Dp427-M isoform of dystrophin (Bladen et al., 2015). The concomitant drastic reduction of the sarcolemmal dystrophin-associated glycoprotein complex causes loss of protein function and is associated with progressive skeletal muscle wasting (Ervasti et al., 1990; Ohlendieck et al., 1993; Murphy and Ohlendieck, 2015). Besides fibre degeneration, key features of muscular dystrophy are disturbed ion homeostasis, abnormal energy metabolism, reactive myofibrosis and adaptive immune responses to chronic muscle damage (Allen et al., 2016; Holland et al., 2016; Tidball et al., 2018; Lindsay et al., 2019). In addition to neuromuscular symptoms, dystrophinopathies are characterized by a multi-system pathology that features respiratory dysfunction, heart failure, scoliosis, metabolic disturbances and cognitive impairments (Goemans and Buyse, 2014; Latimer et al., 2017; Cordova et al., 2018), as well as renal and urinary tract manifestations (Askeland et al., 2013; Bertrand et al., 2016; Braat et al., 2015).

Although cardio-respiratory failure is the main cause of death in Duchenne patients (Moriuchi et al., 1991), the systematic application of cardio-protective drug therapy, including beta-blockers, angiotensin-converting enzyme inhibitors and diuretics to treat cardiac insufficiency (Hor et al., 2018) and mechanical ventilator support to counter-act contractile weakness of respiratory muscles (LoMauro et al., 2015) has

* Corresponding author at: Department of Biology, Maynooth University, National University of Ireland, Maynooth W23F2H6, Co. Kildare, Ireland.
*E-mail address:* kay.ohlendieck@mu.ie (K. Ohlendieck).

https://doi.org/10.1016/j.ejcb.2019.151059
Received 23 July 2019; Received in revised form 8 October 2019; Accepted 15 October 2019

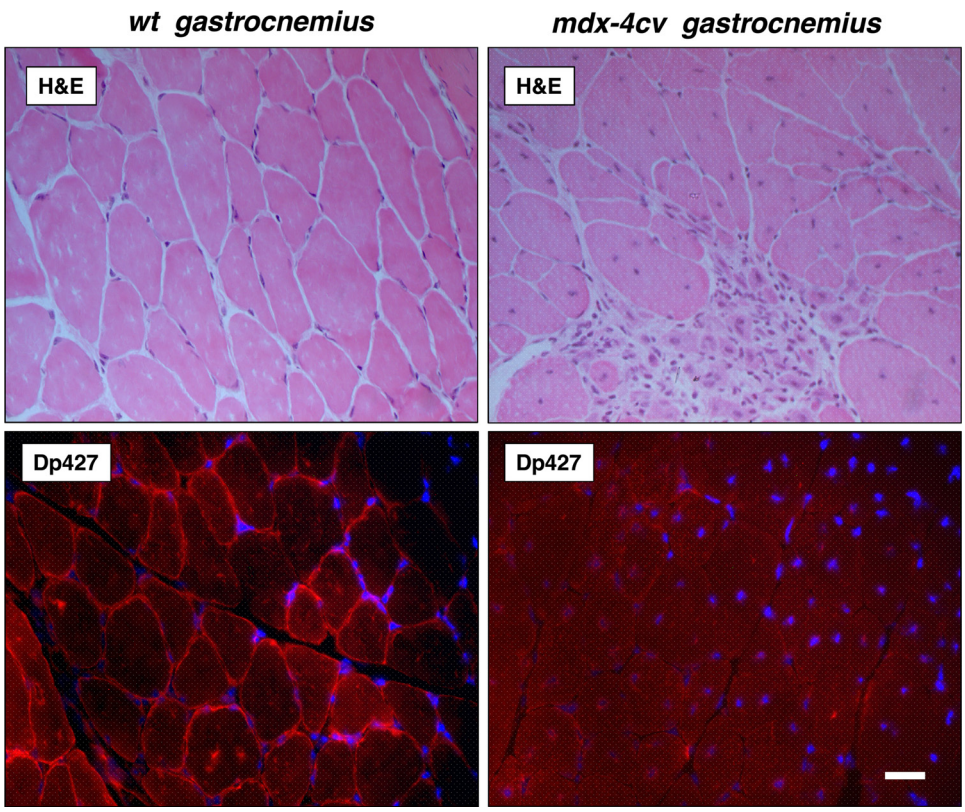


**Fig. 1.** Cell biological characterization of the *mdx-4cv* mouse model of dystrophinopathy. Shown are transverse cryosections of wild type (*wt*) versus dystrophic *mdx-4cv gastrocnemius* muscle stained with haematoxylin and eosin (H &E) and labelled with antibodies to the full-length Dp427 isoform of dystrophin. The dystrophic specimens clearly exhibit the almost complete loss of dystrophin at the sarcolemma, as well as central nucleation, cellular degeneration, inflammation and abnormal fibre diameters. Bar equals 50 µm.

drastically enhanced the prognosis in dystrophinopathy (Messina and Vita, 2018). However, improved life expectancy is associated with an altered rate of circulation due to an extended period of decreased cardiac output and this in turn causes progressive dysfunction in other organ systems. As a serious complication in advanced stages of X-linked muscular dystrophy, contractile weakness was shown to be associated with the cardio-renal syndrome (Villa et al., 2016) and fatal cases of acute renal failure have been described (Matsumura et al., 2012). Non-ambulatory Duchenne patients have an increased risk of symptomatic nephrolithiasis (Shumyatcher et al., 2008; Singh et al., 2007) and reduced kidney perfusion (Motoki et al., 2015), whereby renal dysfunction can be identified and monitored by the Cystatin C-estimated glomerular filtration rate (Villa et al., 2016; Viollet et al., 2009).

Because of these renal abnormalities in dystrophic patients, it was of interest to evaluate potential proteome-wide changes in the kidney in association with dystrophinopathy. However, due to the extremely restricted amounts of patient tissue biopsy material available to study genetic diseases of childhood, animal models have been widely employed to study the molecular pathogenesis of X-linked muscular dystrophy (McGreevy et al., 2015; Rodrigues et al., 2016; Wilson et al., 2017). In analogy, we have used here kidney specimens from the established *mdx-4cv* mouse model of X-linked muscular dystrophy (Banks et al., 2010; Im et al., 1996; Tichy and Mourkioti, 2017). Genetic *mdx*-type mouse models have previously been used for studying cellular abnormalities in the kidney (Gusel'nikova et al., 2018) and the evaluation of kidney toxicity in relation to pharmacological applications (Reay et al., 2015) and experimental exon-skipping therapy (Zhang et al., 2015) to treat muscular dystrophy. Importantly, adult *mdx* mice were shown to exhibit reduced renal function using serum Cystatin C testing and dynamic computed tomography scanning with an angiographic agent (Wada et al., 2019). These renal functional tests have demonstrated the usefulness of *mdx*-type models for screening the kidney from dystrophin-deficient animals. In this report, the systematic proteomic survey of the *mdx-4cv* kidney has revealed the drastic elevation of the FABP1 isoform of fatty acid binding protein (Hotamisligil and Bernlohr, 2015), which may be related to ectopic fat deposition and renal dysfunction (Xu et al., 2015).

## 2. Materials and methods

### 2.1. Materials

General materials and analytical grade reagents were purchased from Sigma Chemical Company (Dorset, UK), Bio-Rad Laboratories (Hemel-Hempstead, Hertfordshire, UK) and GE Healthcare (Little Chalfont, Buckinghamshire, UK). Sequencing grade-modified trypsin, Lys-C and Protease Max Surfactant Trypsin Enhancer were obtained from Promega (Madison, WI, USA). Whatman nitrocellulose transfer membranes and Invitrogen NuPAGE Novex Bis-Tris gels were from Bio-Science Ltd (Dun Laoghaire, Ireland). InstantBlue Coomassie Protein Stain was purchased from Expedeon (Heidelberg, Germany). The chemiluminescence substrate and protease inhibitors were obtained from Roche Diagnostics (Mannheim, Germany). Primary antibodies were from Cell Signaling Technology, Leiden, Netherlands (rabbit mAb13368 to fatty acid binding protein FABP1), Proteintech, Manchester, UK (rabbit pAb 10168-2-AP to the ACSM3 isoform of mitochondrial acyl-coenzyme A synthetase), R&D Systems, Abingdon, UK (mouse mAb MAB5718 to glyceraldehyde-3-phosphate dehydrogenase) and Leica Biosystems, Wetzlar, Germany (mouse mAb NCL-DYS1/clone-Dy8/6C5 to dystrophin). Anti-rabbit and anti-mouse peroxidase conjugated secondary antibodies were from Cell Signaling Technology. For immunofluorescence microscopy, normal goat serum, goat anti-mouse IgG RRX (Rhodamine Red-X) and anti-rabbit Alexa Fluor 488 antibody were purchased from Molecular Probes, Life Technologies (Darmstadt, Germany) and Jackson ImmunoResearch (West Grove, PA, USA), respectively. The embedding medium Fluoromount G was from Southern Biotech (Birmingham, AL, USA).

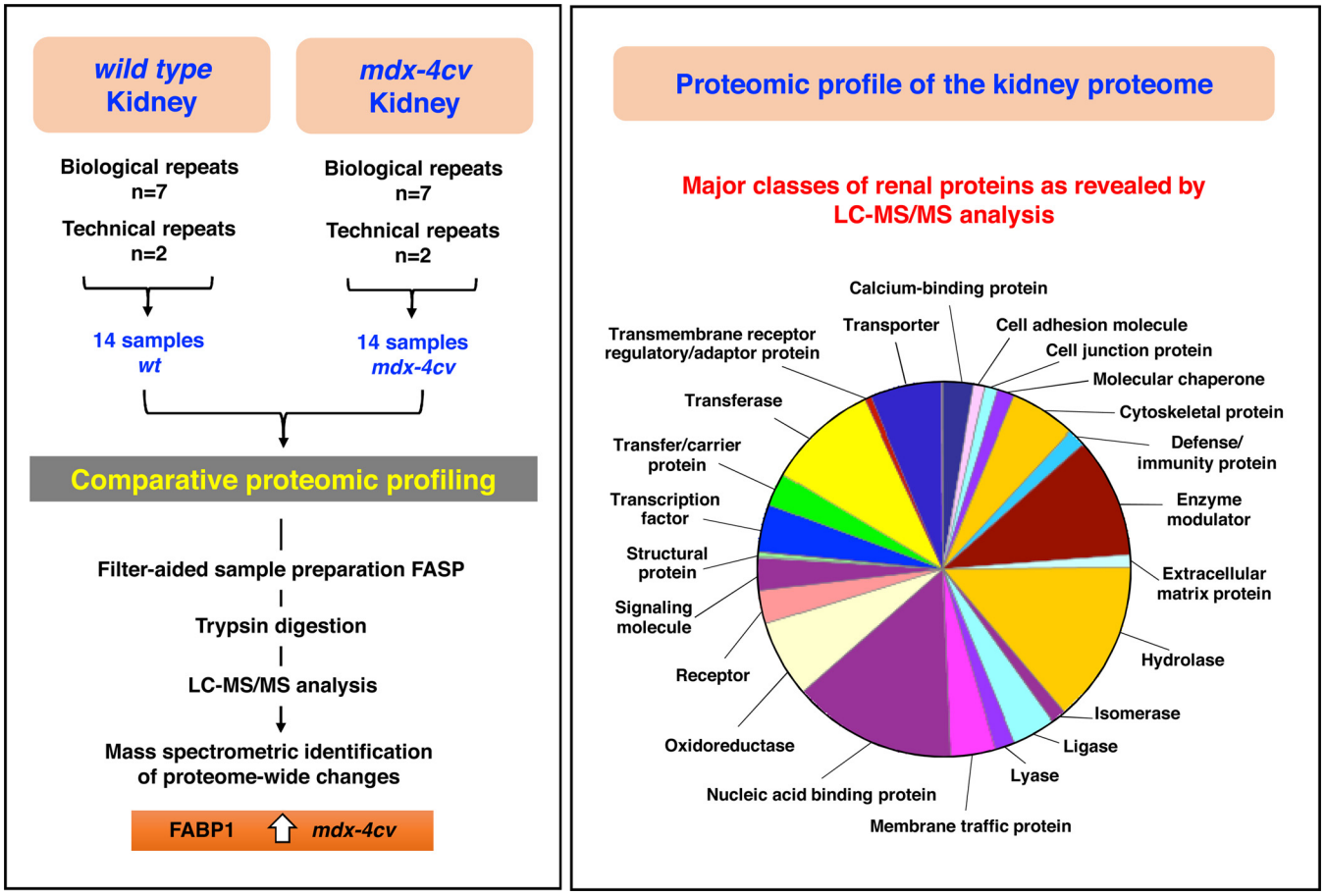


**Fig. 2.** Overview of the comparative proteomic profiling of the kidney from the *mdx-4cv* model of X-linked muscular dystrophy. Shown is the experimental workflow used in the proteomic analysis of 12-month old mouse kidney using an Orbitrap Fusion Tribrid mass spectrometer, as well as the bioinformatic PANTHER analysis of the distribution of protein classes within the assessable kidney proteome.

### *2.2. Preparation of kidney samples from the mdx-4cv mouse model of dystrophinopathy*

For the comparative mass spectrometric profiling of the kidney proteome from dystrophic mice, whole kidney samples from 12-month old *mdx-4cv* mice versus age-matched control C57/BL6 mice were obtained from the Bioresource Unit of the University of Bonn (Murphy et al., 2018a). Mice were kept under standard conditions and all procedures adhered to German legislation on the use of animals in experimental research. The *mdx-4cv* mouse model of Duchenne muscular dystrophy is one of four chemical variants of the spontaneous *mdx* mouse (Partridge, 2013), which has been generated on the C57/BL6 background by chemical mutagenesis (Chapman et al., 1989; Danko et al., 1992; Shin et al., 2011). Mice were sacrificed by cervical dislocation and kidneys were dissected and quick-frozen in liquid nitrogen. Tissue specimens were transported to Maynooth University in accordance with the Department of Agriculture (animal by-product register number 2016/16 to the Department of Biology, National University of Ireland, Maynooth) on dry ice and stored at −80 °C prior to analysis.

For sample preparation, 25 mg of kidney tissue was lysed by homogenisation with 200 µl of lysis solution (4 % SDS, 100 mM Tris-Cl pH7.6, 0.1 M DTT) and incubated at 95 °C for 3 min and then sonicated for 30 s. The lysate was clarified by centrifugation at 16,000xg for 5 min. 10 µl of lysate was mixed with 200 µl of 8 M urea, 0.1 M Tris pH8.9 in filter units (Sartorius, Vivacon 500, Product number: VN0H22) and centrifuged at 14,000xg for 15 min. Samples were subsequently processed according to the standardized FASP protocol for filter-aided sample preparation (Wiśniewski et al., 2009).

### *2.3. Label-free liquid chromatography mass spectrometry*

Reverse-phased capillary high pressure liquid chromatography was carried out using the UltiMate 3000 nano system (Thermo Scientific) coupled directly in-line with the Thermo Orbitrap Fusion Tribrid Mass Spectrometer (Thermo Scientific) (Murphy et al., 2019b). The digested kidney protein samples (1 µl ~ 800 ng peptide) were loaded onto the trapping column (PepMap100, C18, 300 µm ×5 mm) at a flow rate of 25 µl/min with 2 % (v/v) acetonitrile (ACN), 0.1 % (v/v) trifluoroacetic acid (TFA) for 3 min before being resolved onto an analytical column (Acclaim PepMap 100, 75 µm ×50 cm, 3 µm bead diameter column). Peptides were eluted using the following binary gradient; solvent A (0.1 % (v/v) formic acid in LC–MS grade water) and 2–27.5 % solvent B (80 % (v/v) ACN, 0.08 % (v/v) formic acid in LC–MS grade water) for 110 min at a flow rate of 300 nl/min. For peptide ionization, a voltage of 1.9 kV was applied and a capillary temperature of 320 °C was used. Data-dependent acquisition with full scans in the 375–1500 $m/z$ range was performed using an Orbitrap mass analyser with a resolution of 120,000 (at $m/z$ 200), a targeted automatic gain control (AGC) value of 4E + 05 and a maximum injection time of 50 ms. The number of selected precursor ions for fragmentation was determined by the top-speed acquisition algorithm. Selected precursor ions were isolated in the Quadrupole with an isolation width of 1.6 Da. Peptides with a charge state of 2+ to 6+ were analysed and a dynamic exclusion was applied after 60 s. Precursor ions were fragmented using higher energy collision-induced dissociation (HCD) with a normalized collision energy

**Table 1**
Proteomic identification of kidney proteins with an increased abundance in the *mdx-4cv* model of Duchenne muscular dystrophy.

| Accession | Gene name | Description | Unique peptides | Confidence score | Anova (p) | Max fold change |
|---|---|---|---|---|---|---|
| P12710 | Fabp1 | Fatty acid-binding protein FABP1 | 2 | 7.7091 | 0.00015 | 21.89 |
| P32848 | Pvalb | Parvalbumin alpha | 2 | 6.7064 | 0.02782 | 14.41 |
| B1AVD1 | Xpnpep2 | Xaa-Pro aminopeptidase 2 | 7 | 23.6486 | 2.32E-06 | 7.6 |
| E9Q4P1 | Wdfy1 | WD repeat and FYVE domain-containing protein 1 | 2 | 5.9427 | 0.00133 | 7.19 |
| P54869 | Hmgcs2 | Hydroxymethyl-glutaryl-CoA synthase, mitochondrial | 5 | 14.1774 | 8.82E-13 | 5.81 |
| O35490 | Bhmt | Betaine–homocysteine S-methyltransferase 1 | 5 | 17.2183 | 1.50E-08 | 5.54 |
| Q9JIL4 | Pdzk1 | Na(+)/H(+) exchange regulatory cofactor NHE-RF3 | 3 | 15.5914 | 3.02E-09 | 3.74 |
| P49429 | Hpd | 4-hydroxyphenyl-pyruvate dioxygenase | 5 | 16.2034 | 7.00E-08 | 3.28 |
| Q9QZE5 | Copg1 | Coatomer subunit gamma-1 | 2 | 8.01240 | 0.03028 | 3.08 |
| Q9D7G0 | Prps1 | Ribose-phosphate pyrophosphokinase 1 | 2 | 7.3691 | 0.01469 | 3.03 |
| P14246 | Slc2a2 | Solute carrier family 2, facilitated glucose transporter member 2 | 2 | 5.5109 | 0.03283 | 2.97 |
| Q8CIM7 | Cyp2d26 | Cytochrome P450 2D26 | 4 | 12.4466 | 1.23E-07 | 2.69 |
| P01029 | C4b | Complement C4-B | 2 | 8.1508 | 0.03575 | 2.54 |
| Q99K67 | Aass | Alpha-aminoadipic semialdehyde synthase, mitochondrial | 2 | 8.3073 | 0.00120 | 2.47 |
| Q61941 | Nnt | NAD(P) transhydrogenase, mitochondrial | 17 | 58.5686 | 0.00017 | 2.44 |
| Q64374 | Rgn | Regucalcin | 2 | 6.7339 | 0.00064 | 2.43 |
| P32067 | Ssb | Lupus La protein homolog | 2 | 8.5021 | 0.02163 | 2.31 |
| O35728 | Cyp4a14 | Cytochrome P450 4A14 | 5 | 17.0102 | 5.95E-05 | 2.3 |
| P70691 | Ugt1a2 | UDP-glucuronosyl-transferase 1-2 | 6 | 24.0153 | 0.00813 | 2.22 |
| P00493 | Hprt1 | Hypoxanthine-guanine phosphoribosyl-transferase | 5 | 22.8354 | 9.56E-10 | 2.21 |
| O35381 | Anp32a | Acidic leucine-rich nuclear phosphoprotein 32 family member A | 2 | 6.4504 | 6.65E-05 | 2.18 |
| P07356 | Anxa2 | Annexin A2 | 2 | 7.5966 | 0.01914 | 2.18 |
| P05063 | Aldoc | Fructose-bisphosphate aldolase C | 2 | 5.5440 | 0.00796 | 2.15 |
| P0DP27 | Calm2 | Calmodulin-2 | 2 | 6.7473 | 0.00084 | 2.1 |
| Q8VBW8 | Ttc36 | Tetratricopeptide repeat protein 36 | 3 | 11.1460 | 2.55E-07 | 2.08 |
| Q9Z2V4 | Pck1 | Phosphoenolpyruvate carboxykinase, cytosolic | 4 | 11.8760 | 1.65E-06 | 1.99 |
| B2RX12 | Abcc3 | Canalicular multispecific organic anion transporter 2 | 2 | 6.8818 | 0.02221 | 1.98 |
| Q91W43 | Gldc | Glycine dehydrogenase (decarboxylating), mitochondrial | 5 | 22.2066 | 0.00021 | 1.97 |
| A6 × 935 | Itih4 | Inter alpha-trypsin inhibitor, heavy chain 4 | 3 | 11.1462 | 0.00140 | 1.94 |
| P62814 | Atp6v1b2 | V-type proton ATPase subunit B, brain isoform | 4 | 16.0112 | 0.00024 | 1.91 |
| Q8CFA2 | Amt | Aminomethyltransferase, mitochondrial | 2 | 5.4561 | 7.21E-08 | 1.89 |
| P11679 | Krt8 | Keratin, type II cytoskeletal 8 | 2 | 6.0165 | 0.00304 | 1.87 |
| Q8VCW8 | Acsf2 | Acyl-CoA synthetase family member 2, mitochondrial | 3 | 16.8266 | 0.00140 | 1.83 |
| Q99JW2 | Acy1 | Aminoacylase-1 | 9 | 25.7654 | 1.55E-06 | 1.79 |
| Q9JK42 | Pdk2 | [Pyruvate dehydrogenase (acetyl-transferring)] kinase isozyme 2, mitochondrial | 2 | 8.4047 | 4.11E-07 | 1.76 |
| P56402 | Aqp2 | Aquaporin-2 | 2 | 6.6277 | 0.03090 | 1.76 |
| P06797 | Ctsl | Cathepsin L1 | 2 | 9.3236 | 2.98E-05 | 1.73 |
| P08905 | Lyz2 | Lysozyme C-2 | 3 | 12.0437 | 2.92E-06 | 1.71 |
| P24549 | Aldh1a1 | Retinal dehydrogenase 1 | 5 | 19.2361 | 2.75E-06 | 1.69 |
| O08691 | Arg2 | Arginase-2, mitochondrial | 3 | 10.7187 | 0.02066 | 1.68 |
| Q6A4L0 | Slc22a13 | Solute carrier family 22 member 13 | 2 | 7.0632 | 0.00970 | 1.64 |
| Q9QXD6 | Fbp1 | Fructose-1,6-bisphosphatase 1 | 4 | 21.5767 | 2.12E-07 | 1.63 |
| Q9D819 | Ppa1 | Inorganic pyrophosphatase | 2 | 9.2567 | 0.00317 | 1.62 |
| Q3V0K9 | Pls1 | Plastin-1 | 2 | 7.3772 | 1.21E-05 | 1.61 |
| O35409 | Folh1 | Glutamate carboxypeptidase 2 | 2 | 10.0178 | 0.00328 | 1.58 |
| A2ATU0 | Dhtkd1 | Probable 2-oxoglutarate dehydrogenase E1 component DHKTD1, mitochondrial | 4 | 10.3485 | 0.00207 | 1.57 |
| Q6PDN3 | Mylk | Myosin light chain kinase, smooth muscle | 4 | 11.6538 | 0.00332 | 1.57 |
| Q6AW69 | Cgnl1 | Cingulin-like protein 1 | 2 | 6.4156 | 0.00656 | 1.56 |
| Q8K2I4 | Manba | Beta-mannosidase | 4 | 12.0985 | 0.00030 | 1.56 |
| Q9QXD1 | Acox2 | Peroxisomal acyl-coenzyme A oxidase 2 | 12 | 36.8270 | 4.51E-06 | 1.55 |
| P58137 | Acot8 | Acyl-coenzyme A thioesterase 8 | 2 | 7.6040 | 0.00046 | 1.53 |
| Q9WVT6 | Ca14 | Carbonic anhydrase 14 | 2 | 5.38492 | 1.46E-06 | 1.52 |
| P62137 | Ppp1ca | Serine/threonine-protein phosphatase PP1-alpha catalytic subunit | 2 | 5.8612 | 0.02301 | 1.52 |
| A2AKK5 | Acnat1 | Acyl-coenzyme A amino acid N-acyltransferase 1 | 5 | 17.7123 | 0.00359 | 1.51 |
| Q60825 | Slc34a1 | Sodium-dependent phosphate transport protein 2A | 5 | 21.4317 | 4.84E-05 | 1.5 |

of 28 %, and resulting MS/MS ions were measured in the linear ion trap. The typical MS/MS scan conditions were as follows: a targeted AGC value of 2E + 04 and a maximum fill time of 35 ms.

### 2.4. Data analysis

Mass spectrometric files (.raw) were first searched qualitatively against the UniProtKB-SwissProt *Mus musculus* database using Proteome Discoverer 1.4 (Thermo Fisher) and Sequest HT (SEQUEST HT algorithm, licence Thermo Scientific, registered trademark University of Washington, USA). The following settings were used: (i) peptide mass tolerance set to 10 ppm, (ii) MS/MS mass tolerance set to 0.02 Da, (iii) a maximum of two missed cleavages, (iv) carbamidomethylation set as a fixed modification (v) methionine oxidation set as a variable modification and (vi) peptide confidence set to high. Subsequently Progenesis QI for Proteomics software (version 3.1; Non-Linear Dynamics, a Waters company, Newcastle upon Tyne, UK) was used for the quantitative analysis of kidney proteins from wild type versus *mdx-4cv* mice. A reference run was selected and all other runs were aligned to this run, thus allowing for any drift in retention time (Murphy et al., 2019b). Prior to being exported as a MASCOT generic file (mgf) to Proteome Discoverer 2.1 (Thermo Scientific) the MS/MS data files were filtered using the following settings: (i) peptide features with ANOVA ≤ 0.01 between experimental groups, (ii) mass peaks with charge states from +1 to +5 and (iii) greater than one isotope per peptide. Protein identification was performed using Proteome Discoverer 2.1 against Mascot (version 2.3, Matrix Science, Boston, MA, USA) and Sequest HT using the UniProtKB-SwissProt *Mus musculus* database. The following search parameters were used: (i) peptide mass tolerance set to 10 ppm, (ii) MS/MS mass tolerance set to 0.02 Da, (iii)

**Table 2**
Proteomic identification of kidney proteins with a decreased abundance in the *mdx-4cv* model of Duchenne muscular dystrophy.

| Accession | Gene name | Description | Unique peptides | Confidence score | Anova (p) | Max fold change |
|---|---|---|---|---|---|---|
| Q3UNX5 | Acsm3 | Acyl-coenzyme A synthetase ACSM3, mitochondrial | 3 | 10.8408 | 0.04215 | 138.93 |
| P97872 | Fmo5 | Dimethylaniline monooxygenase [N-oxide-forming] 5 | 3 | 10.1945 | 0.01630 | 103.18 |
| P28665 | Mug1 | Murinoglobulin-1 | 6 | 28.5659 | 0.00010 | 3.52 |
| P15392 | Cyp2a4 | Cytochrome P450 2A4 | 3 | 9.1835 | 5.67E-06 | 3.46 |
| P57016 | Lad1 | Ladinin-1 | 3 | 10.7561 | 1.36E-08 | 2.96 |
| P11087 | Col1a1 | Collagen alpha-1(I) chain | 2 | 7.9578 | 1.76E-06 | 2.24 |
| Q01149 | Col1a2 | Collagen alpha-2(I) chain | 4 | 12.6703 | 1.54E-07 | 2.19 |
| Q8C0I1 | Agps | Alkyldihydroxyacetone-phosphate synthase, peroxisomal | 5 | 17.3564 | 0.00039 | 2.02 |
| Q7TNG8 | Ldhd | D-lactate dehydrogenase, mitochondrial | 3 | 7.2202 | 0.00032 | 1.98 |
| Q9JI33 | Ntn4 | Netrin-4 | 2 | 7.6159 | 9.74E-08 | 1.93 |
| O55029 | Copb2 | Coatomer subunit beta | 2 | 7.0038 | 0.00228 | 1.91 |
| P01872 | Ighm | Immunoglobulin heavy constant mu | 3 | 8.1050 | 0.03329 | 1.91 |
| Q9JK53 | Prelp | Prolargin | 2 | 5.5677 | 2.66E-06 | 1.87 |
| O89053 | Coro1a | Coronin-1A | 2 | 7.6804 | 0.00034 | 1.83 |
| Q02788 | Col6a2 | Collagen alpha-2(VI) chain | 8 | 26.2823 | 1.06E-07 | 1.78 |
| Q9DC50 | Crot | Peroxisomal carnitine O-octanoyltransferase | 2 | 5.3420 | 0.02421 | 1.76 |
| Q91WV7 | Slc3a1 | Neutral and basic amino acid transport protein rBAT | 2 | 5.4986 | 0.01564 | 1.73 |
| Q64FW2 | Retsat | All-trans-retinol 13,14-reductase | 3 | 8.6878 | 1.13E-05 | 1.72 |
| P47740 | Aldh3a2 | Fatty aldehyde dehydrogenase | 3 | 7.5906 | 0.02707 | 1.69 |
| P50172 | Hsd11b1 | Corticosteroid 11-beta-dehydrogenase isozyme 1 | 4 | 11.6482 | 0.00010 | 1.68 |
| Q8VC12 | Uroc1 | Urocanate hydratase | 6 | 20.4403 | 0.00169 | 1.67 |
| P20918 | Plg | Plasminogen | 2 | 6.05155 | 0.00137 | 1.66 |
| Q9JJU8 | Sh3bgrl | SH3 domain-binding glutamic acid-rich-like protein | 2 | 5.6793 | 5.00E-05 | 1.65 |
| Q08857 | Cd36 | Platelet glycoprotein 4 | 2 | 6.1668 | 0.00043 | 1.65 |
| P00329 | Adh1 | Alcohol dehydrogenase 1 | 2 | 5.1563 | 0.03316 | 1.64 |
| P43276 | Hist1h1b | Histone H1.5 | 2 | 6.5163 | 7.05E-05 | 1.63 |
| Q9WU78 | Pdcd6ip | Programmed cell death 6-interacting protein | 2 | 6.4367 | 0.00077 | 1.62 |
| Q9R0H0 | Acox1 | Peroxisomal acyl-coenzyme A oxidase 1 | 2 | 4.3429 | 0.01386 | 1.6 |
| P07758 | Serpina1a | Alpha-1-antitrypsin 1-1 | 3 | 14.9066 | 1.65E-05 | 1.59 |
| Q99K41 | Emilin1 | EMILIN-1 | 2 | 7.63098 | 0.00167 | 1.53 |
| Q04857 | Col6a1 | Collagen alpha-1(VI) chain | 4 | 10.5504 | 1.74E-08 | 1.53 |

up to two missed cleavages, (iv) carbamidomethylation set as a fixed modification and (v) methionine oxidation set as a variable modification. For re-importation back into Progenesis LC−MS software as a PepXML file only peptides with either ion scores of 40.00 or more (from Mascot) and peptides with XCorr scores ≥ 1.5 (from Sequest HT) were allowed. The following criteria were applied to assign proteins as positively identified: (i) an ANOVA score between experimental groups of ≤0.01, and (ii) proteins with ≥2 peptides matched. The freely available software packages PANTHER (Mi et al., 2017; http://pantherdb.org/) and STRING (Szklarczyk et al., 2017; https://string-db.org/) were used to identify protein classes and characterise potential protein interactions, respectively.

### 2.5. Comparative immunoblot analysis

Immunoblotting was used as an orthogonal method for the independent verification of changes in newly identified proteins in the kidney of the *mdx-4cv* mouse model of dystrophinopathy (Murphy et al., 2019a). Individual protein samples (12.5 µg protein per lane for Coomassie staining; and 25 µg protein per lane for immunoblotting) were run on NuPAGE Novex Bis-Tris Gels (Invitrogen) under standard conditions. Protein concentration was determined using the Bradford assay system (Bradford, 1976). For comparative analyses, Coomassie staining of protein gels was carried out with InstantBlue Coomassie Protein Stain (Expedeon). Proteins were transferred to nitrocellulose membranes, blocked and incubated with primary antibody overnight, followed by detection with peroxidase-conjugated secondary antibodies using the enhanced chemiluminescence method. Densitometric scanning and statistical analysis of immunoblots was performed using a HP PSC-2355 scanner and ImageJ software (NIH, Bethesda, MD, USA) along with Microsoft excel in which statistical significance was based on a p-value ≤ 0.05.

### 2.6. Comparative histology and immunofluorescence microscopy

In order to establish the loss of the skeletal muscle dystrophin isoform Dp427-M in the *mdx-4cv* mouse model of dystrophinopathy and correlate it to potential changes in the kidney, histological haematoxylin and eosin staining, as well as immunofluorescence microscopy were carried out by standardized methodology. Freshly dissected kidney and skeletal muscle specimens from 12-month old wild type and *mdx-4cv* mice were quick-frozen in liquid nitrogen-cooled isopentane and 10 µm sections cut in a cryostat. For dystrophin immuno-staining, unfixed cryosections were boiled in phosphate-buffered saline for 5 min as previously described in detail (Murphy et al., 2019b). For FABP1 and ACSM3 staining, sections were fixed in a 1:1 (v/v) mixture of methanol and acetone for 10 min at room temperature and then blocked with 1:20 diluted normal goat serum for 30 min at room temperature. Primary antibodies were diluted appropriately in phosphate-buffered saline for overnight incubation at 4 °C. Tissue specimens were carefully washed and then incubated with fluorescently-labelled secondary antibodies, using either 1:200 diluted anti-rabbit Alexa Fluor 488 antibody or 1:200 diluted anti-mouse RRX antibody for 45 min at room temperature. Nuclei were counter-stained with 1 µg/ml bis-benzimide Hoechst 33,342. Antibody-labelled kidney and muscle tissue sections were embedded in Fluoromount G medium and viewed under a Zeiss Axioskop 2 epifluorescence microscope equipped with a digital Zeiss AxioCam HRc camera (Carl Zeiss Jena GmbH, Jena, Germany).

For Sudan Black staining, fresh kidney tissue sections were fixed in 10 % formalin, washed under tap water, rinsed with distilled water and then exposed twice for 5 min to propylene glycol. Incubation with Sudan Black B (0.7 g dye in 100 ml propylene glycol) was carried out for 7 min with agitation, followed by 3 min in 85 % propylene glycol, rinsing with distilled water, washing with tap water, another rinsing step with distilled water and finally mounting in an aqueous mounting media of glycerin jelly.

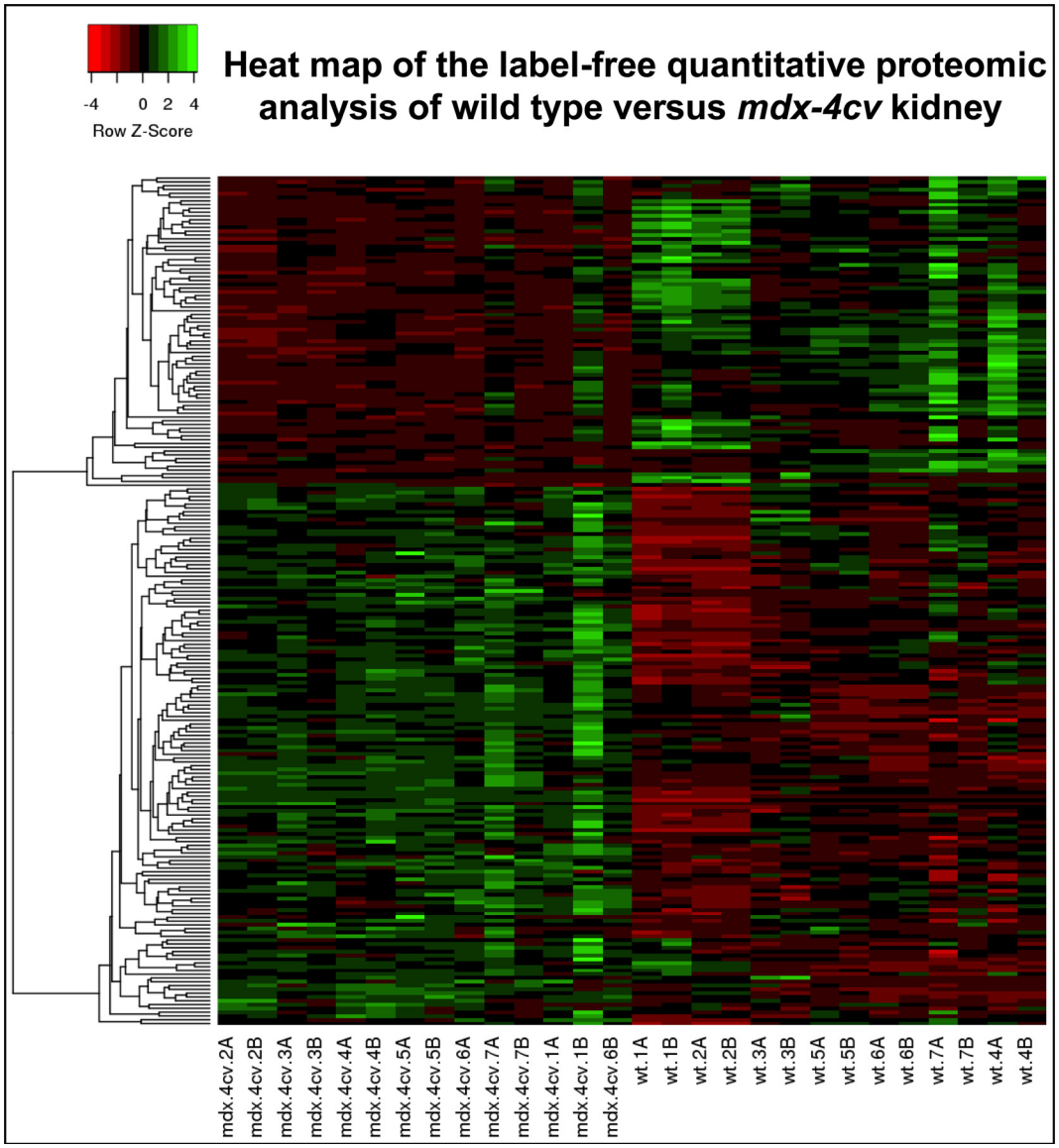


**Fig. 3.** Label-free quantitative proteomic analysis of wild-type versus *mdx-4cv* kidney. Depicted is the result from hierarchical clustering of the mean protein expression values of statistically significant differentially abundant proteins.

## 3. Results

Since X-linked muscular dystrophy is associated with renal dysfunction, it was of interest to perform a proteomic survey of the kidney from the dystrophic *mdx-4cv* mouse. Prior to the mass spectrometric analysis of kidney extracts, the dystrophic and mutant status of the genetic mouse model of dystrophinopathy was established by histological analysis and immunofluorescence microscopy. Fig. 1 shows transverse cryosections from *gastrocnemius* muscle and confirms abnormal fibre diameters, central nucleation, cellular degeneration and inflammation in *mdx-4cv* skeletal muscle, as well as the loss of dystrophin isoform Dp427-M at the fibre periphery.

### 3.1. Proteomic profiling of mouse kidney

A crucial prerequisite for the biochemical establishment of proteome-wide changes in the kidney from the *mdx-4cv* model of X-linked muscular dystrophy is the comprehensive coverage of the experimentally assessable protein complement from total kidney extracts. The proteomic analysis of 12-month old mouse kidney using an Orbitrap Fusion Tribrid mass spectrometer, presented in this report, is based on the mass spectrometric identification of 5878 renal protein species. The bioinformatics PANTHER analysis of the distribution of protein classes within the assessable kidney proteome is presented in Fig. 2, in addition to the bioanalytical workflow used for the analysis of the *mdx-4cv* kidney. Tables listing the most abundant kidney proteins identified by proteomics, as well as kidney marker proteins with characteristic tissue distributions and physiological functions are provided in an accompanying Data-in-Brief manuscript (Dowling et al., 2019). The multi-consensus file of mouse kidney, which forms the basis of this study, is available through the Open Science Framework under the project title 'Proteomic profiling of mouse kidney' (Dowling et al., 2019). The file includes data from the analysis of 28 separate mass spectrometric sample runs (2 technical repeats of 14 biological repeats) consisting of high confidence peptides that were filtered based on Xcorr values. The identified spectrum of kidney-associated proteins ranged from small proteins (alpha-B-crystallin of 22 kDa; 9 unique peptides, 62 % sequence coverage) to medium-size proteins (endoplasmic reticulum calcium ATPase SERCA2 of 115 kDa; 43 unique peptides, 46 % sequence coverage) to very large proteins (cytoplasmic dynein heavy chain of 532 kDa; 184 unique peptides, 50 % sequence coverage).

A wide range of kidney-associated proteins, as previously

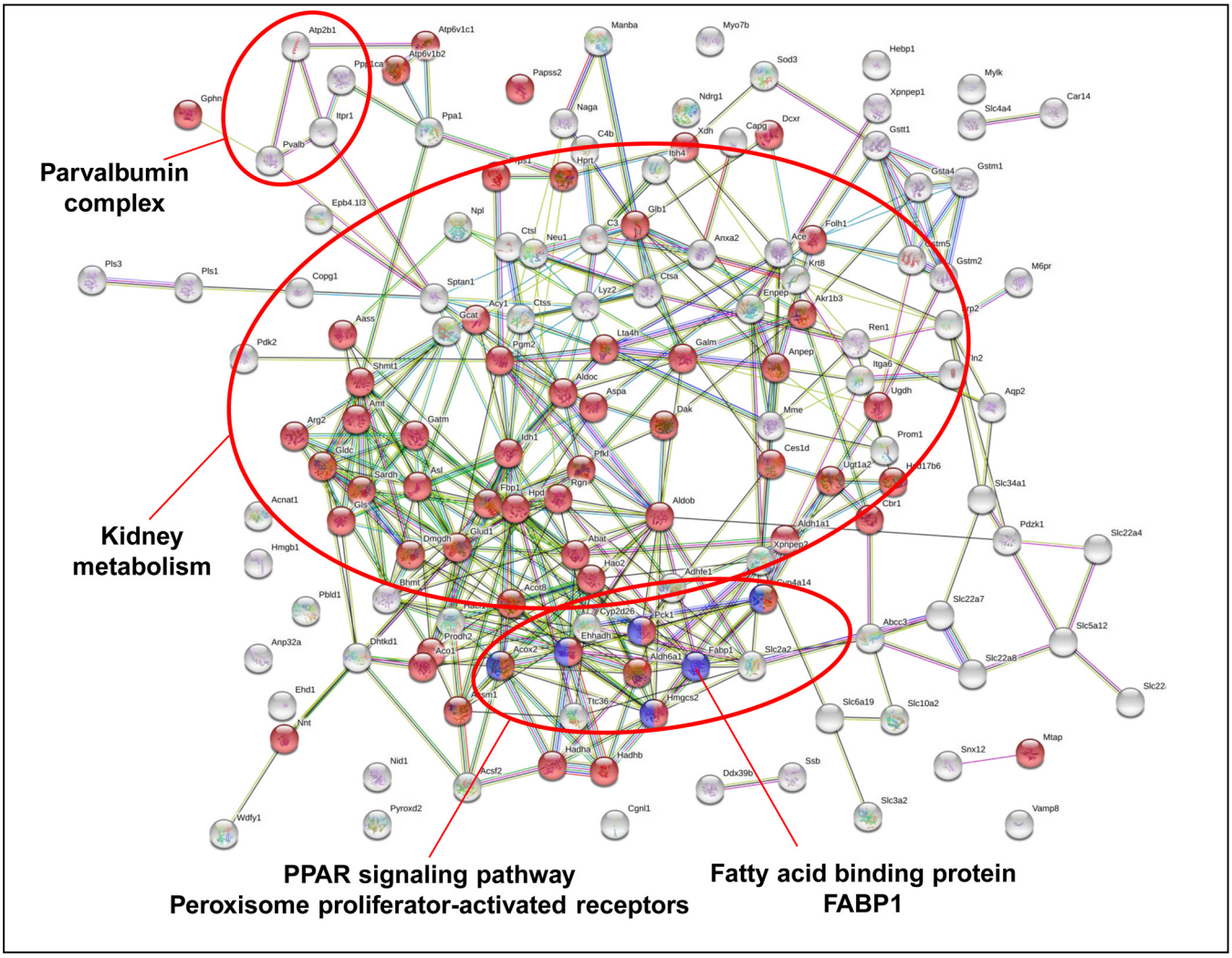


**Fig. 4.** Overview of potential protein-protein interaction patterns of increased protein species in the kidney from the *mdx-4cv* mouse model of dystrophinopathy, as determined by the bioinformatics software programme STRING.

established by antibody-based methodology (Habuka et al., 2014), were identified with solid sequence coverage including renal marker proteins belonging to the glomeruli (podocin; 4 unique peptides, 18 % sequence coverage), the proximal tubule cytoplasm (inositol oxygenase; 12 unique peptides, 74 % sequence coverage), the proximal tubule basolateral membrane (solute carrier SLC22A2; 5 unique peptides, 10 % sequence coverage), the proximal tubule luminal membrane (solute carrier SLC22A12; 12 unique peptides, 19 % sequence coverage), the distal tubule luminal membrane (ATP-sensitive inward rectifier potassium channel KCNJ1; 3 unique peptides, 10 % sequence coverage) and the collecting duct luminal membrane (aquaporin AQP2; 3 unique peptides, 13 % sequence coverage). A highly specific kidney marker protein is uromodulin, which is exclusively produced by epithelial cells in the thick ascending limb cells of the kidney, where it regulates ion transport, as well as protects via immunomodulation against urinary tract infection and kidney stones (Garimella and Sarnak, 2017). Uromodulin (Q91 X17; *Umod* gene product), was identified by 18 unique peptides and a 33 % sequence coverage in all analysed 28 kidney samples. Another type of highly kidney-enriched proteins is the diverse family of solute carriers that regulate specific aspects of renal transmembrane transport in the proximal and distal tubule system and the collecting ducts (Momper and Nigam, 2018). The kidney-enriched solute carriers SLC12A1 (SLC family 12, member 1; 33 unique peptides; 40 % sequence coverage) and SLC22A8 (SLC family 22, member 8; 10 unique peptides, 20 % sequence coverage) were clearly identified in this study, together with 38 other isoforms of this protein family of solute carriers (Habuka et al., 2014).

Key regulators involved in kidney physiology are represented by the $Na^+/Ca^{2+}$-exchanger, the $Na^+$/glucose-cotransporter and the plasmalemmal membrane $Ca^{2+}$-ATPase, as well as the highly abundant renal $Na^+/K^+$-ATPase (Xie et al., 2013). Various isoforms of these kidney marker proteins were covered by the proteomic profiling presented in this study, including the $Na^+/Ca^{2+}$-exchangers NCX1 (5 unique peptides; 6 % sequence coverage) and NCX2 (2 unique peptides; 4 % sequence coverage), the $Na^+$/glucose-cotransporters SGLT1 (13 unique peptides; 22 % sequence coverage), SGLT2 (10 unique peptides; 16 % sequence coverage), SGLT4 (8 unique peptides; 18 % sequence coverage) and SGLT5 (8 unique peptides; 20 % sequence coverage), the plasma membrane $Ca^{2+}$-transporting ATPases ATP2B1 (27 unique peptides; 30 % sequence coverage) and ATP2B4 (22 unique peptides; 25 % sequence coverage) and the $Na^+/K^+$-ATPase subunits alpha-1 (ATP1A1; 47 unique peptides; 50 % sequence coverage), alpha-2 (ATP1A2; 17 unique peptides; 21 % sequence coverage), alpha-3 (ATP1A3; 17 unique peptides; 24 % sequence coverage), beta-1 (ATP1B1; 15 unique peptides; 52 % sequence coverage) and beta-3 (ATP1B3; 4 unique peptides; 19 % sequence coverage). These findings demonstrate an excellent coverage of the assessable proteome from kidney homogenates (Arthur et al., 2018; Cañadas-Garre et al., 2019; Klein and Schanstra, 2018).

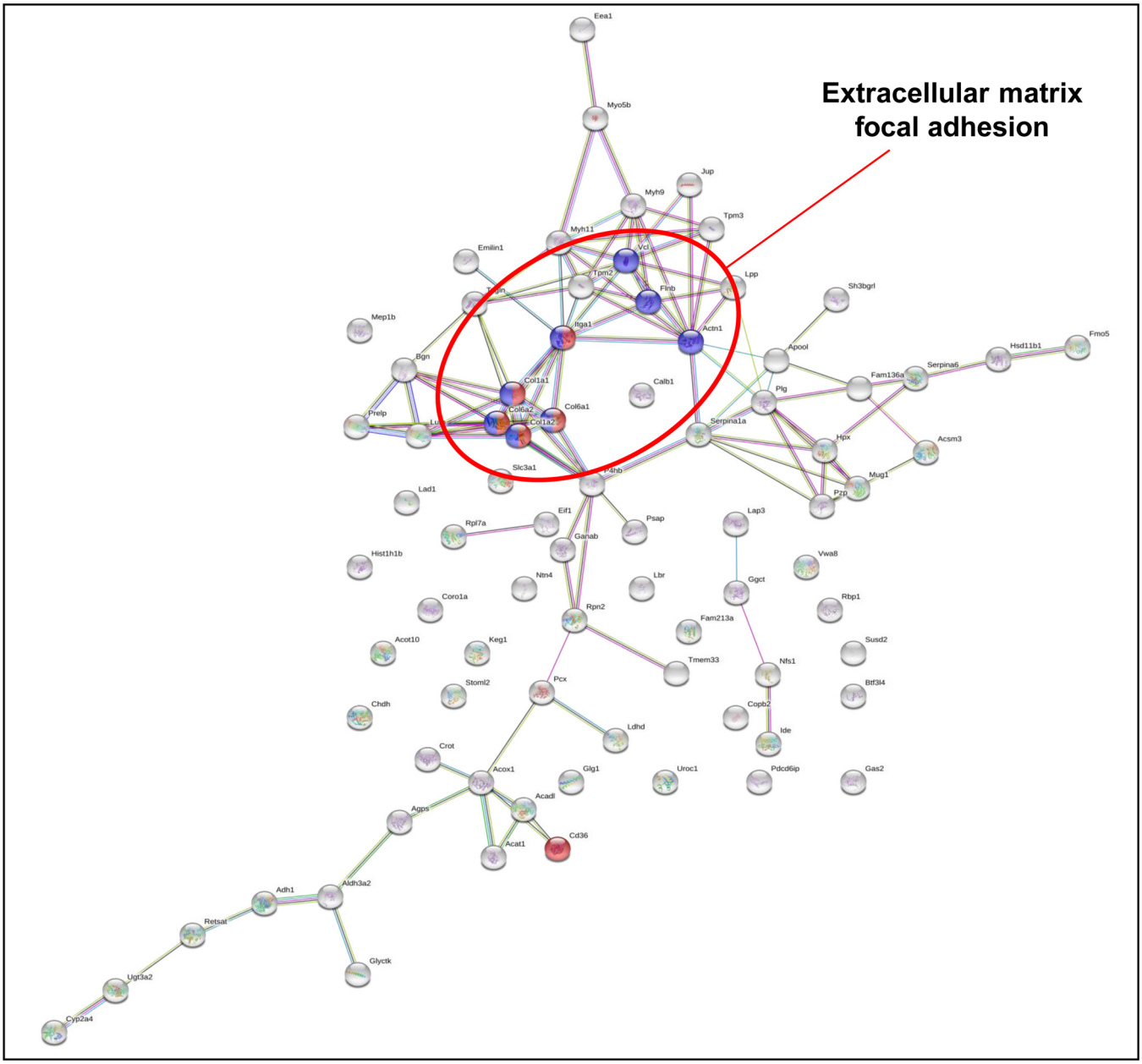


**Fig. 5.** Overview of potential protein-protein interaction patterns of decreased protein species in the kidney from the *mdx-4cv* mouse model of dystrophinopathy, as determined by the bioinformatics software programme STRING.

### 3.2. Comparative proteomic profiling of the mdx-4cv kidney

The comparative mass spectrometric analysis of wild type versus the *mdx-4cv* mouse model of Duchenne muscular dystrophy resulted in the identification of 82 decreased versus 142 increased kidney proteins. The mass spectrometric identification of individual proteins with a changed concentration above 1.5 fold is listed in Table 1 for increased protein species and in Table 2 for decreased protein species, respectively. Tables listing identified kidney proteins with concentration changes below 1.5 fold are provided in an accompanying Data-in-Brief manuscript (Dowling et al., 2019). A summarizing heat map for differentially abundant kidney proteins is shown in Fig. 3. The most increased versus decreased protein species are the FABP1 isoform of fatty acid binding protein versus the ACSM3 isoform of mitochondrial acyl-coenzyme A synthetase, respectively. The list of elevated kidney components contains crucial proteins involved in $Ca^{2+}$-homeostasis (parvalbumin, regucalcin, annexin, calmodulin), and kidney metabolism, including various mitochondrial enzymes (hydroxymethyl-glutaryl-CoA synthase, alpha-aminoadipic semialdehyde synthase, NAD(P) transhydrogenase, glycine dehydrogenase, aminomethyltransferase, acyl-CoA synthetase, pyruvate dehydrogenase kinase, arginase and 2-oxoglutarate dehydrogenase).

The STRING analysis shown in Fig. 4 illustrates the potential interaction patterns of proteins with an increased abundance in the *mdx-4cv* kidney. Highlighted is the parvalbumin complex, the large constellation of metabolic enzymes, the peroxisome proliferation-activated receptor pathway and coupling to FABP1. A striking cluster of decreased proteins is related to the extracellular matrix and focal adhesion complex, as outlined in the STRING analysis of Fig. 5. Significantly reduced proteins in the *mdx-4cv* kidney include the alpha-1(I), alpha-2(I) chain, alpha-1(VI) and alpha-2(VI) chains of collagen, as well as the leucine-rich repeat protein prolargin and the basement membrane components ladinin and netrin. The main proteomic findings were confirmed by immunofluorescence microscopy and comparative

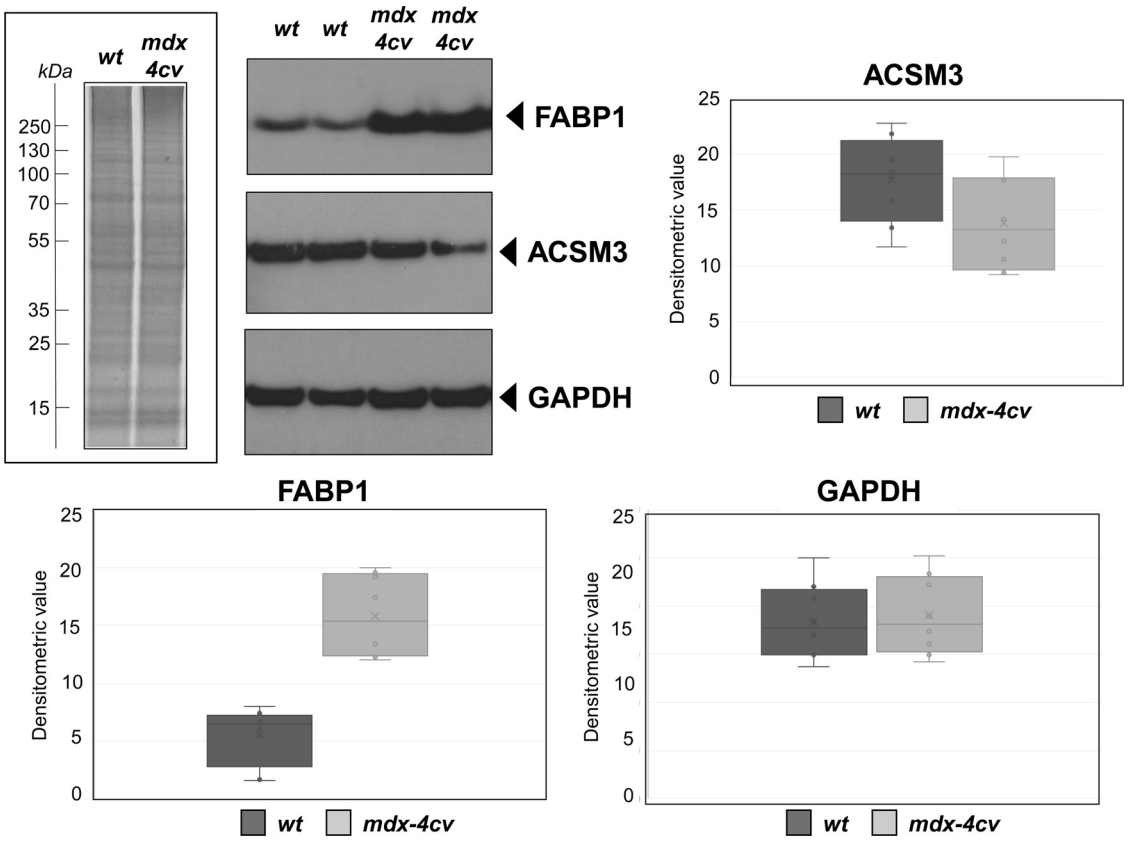


**Fig. 6.** Immunoblot analysis of fatty acid binding protein FABP1 and the ACSM3 isoform of mitochondrial acyl-coenzyme A synthetase in kidney preparations from wild type versus dystrophic mice. Shown is a protein gel of wild type (*wt*) versus *mdx-4cv* kidney extracts, and immunoblots of two separate preparations labelled with antibodies to FABP1, ACSM3 and glyceraldehyde-3-phosphate dehydrogenase (GAPDH). The statistical evaluation of antibody labelling is shown to the right and below the immunoblotting images (FABP1: p = 1.173E-05, n = 7; ACSM3: p = 0.0779, n = 7; GAPDH: p = 0.747, n = 7).

immunoblotting, as outlined below.

### 3.3. Elevated FABP1 levels and ectopic fat depositions in the mdx-4cv kidney

Of the 10 known FABP isoforms (Smathers and Petersen, 2011), 4 variants were identified in this study. FABP1 (L-FABP), FABP3 (H-FABP), FABP4 (A-FABP) and FABP5 (E-FABP) were identified by 5, 7, 8 and 9 unique peptides, respectively. Comparative proteomics indicates that the kidney-associated FABP1 isoform exhibits an approximately 20-fold increased concentration in the dystrophic phenotype (Table 1). Immunoblot analysis was used to verify this finding. As shown in the protein gel of Fig. 6, the overall protein band pattern is relatively comparable between wild type and *mdx-4cv* kidneys. However, immunoblotting clearly revealed that FABP1 is significantly increased in *mdx-4cv* kidney preparations, as compared to reduced levels of ACSM3 and unchanged levels of the glyceraldehyde-3-phosphate dehydrogenase protein product of the house keeping gene *GAPDH*. The elevated concentration of FABP1, as determined by proteomics and confirmed by immunoblotting, was correlated to cell biological changes using histological and immunofluorescence microscopical methodology. The basic histological structure of glomerulus and convoluted tubules was stained by haematoxylin and eosin (Fig. 7). The comparison of kidney sections from wild type versus *mdx-4cv* mice showed increased levels of diffuse whitish deposits in the *mdx-4cv* kidney. Importantly, an increased intensity of Sudan Black labelling of kidney cells revealed ectopic fat deposition. Antibody labelling of FABP1 confirmed increased levels of this fatty acid binding protein in the *mdx-4cv* kidney, as well as a decreased concentration of the ACSM3 isoform of mitochondrial acyl-coenzyme A synthetase (Fig. 7).

## 4. Discussion

The identification and characterization of novel biomarker candidates is crucial for the improved diagnosis, prognosis and therapy-monitoring in the field of muscular dystrophy (Hathout et al., 2016; Carr et al., 2018; Spitali et al., 2018), giving mass spectrometry-based proteomics a central place in the systems biological study of dystrophinopathy (Burch et al., 2015; Dowling et al., 2019). The comprehensive biochemical analysis of proteome-wide changes in the *mdx-4cv* mouse promises to identify novel biomarker candidates, which may be useful for future evaluations of new experimental therapies. The devastating effects of muscular dystrophy are complicated by physiological and biochemical disturbances of whole body homeostasis and the fact that the tissue-specific expression of dystrophin isoforms is driven by seven promoters that independently produce Dp427-B in the brain, Dp427-M contractile tissues, Dp427-P in Purkinje cells, Dp260-R in the retina, Dp140-B/K in brain and kidney, Dp116-S in Schwann cells und the ubiquitous Dp71-G in the brain and various other tissues (Muntoni et al., 2003). Thus, genetic rearrangements in the 79 exon-spanning *DMD* gene have complex effects on the expression of the various dystrophin isoforms in individual cases of muscular dystrophy. Here, we could show that the *mdx-4cv* animal model of dystrophinopathy exhibits considerable changes in the kidney proteome. In analogy to previous findings from the systematic proteomic analysis of this dystrophic mouse model on fibre degeneration and reactive myofibrosis (Holland et al., 2015; Murphy et al., 2018a, 2019a, 2019b), this report confirms the multi-system pathology due to deficiency in dystrophin.

Kidney proteomics and kidney disease biomarker research has greatly intensified over the last few years, as outlined in several extensive reviews (Fenton, 2018; Rysz et al., 2017; Zhang and Parikh,

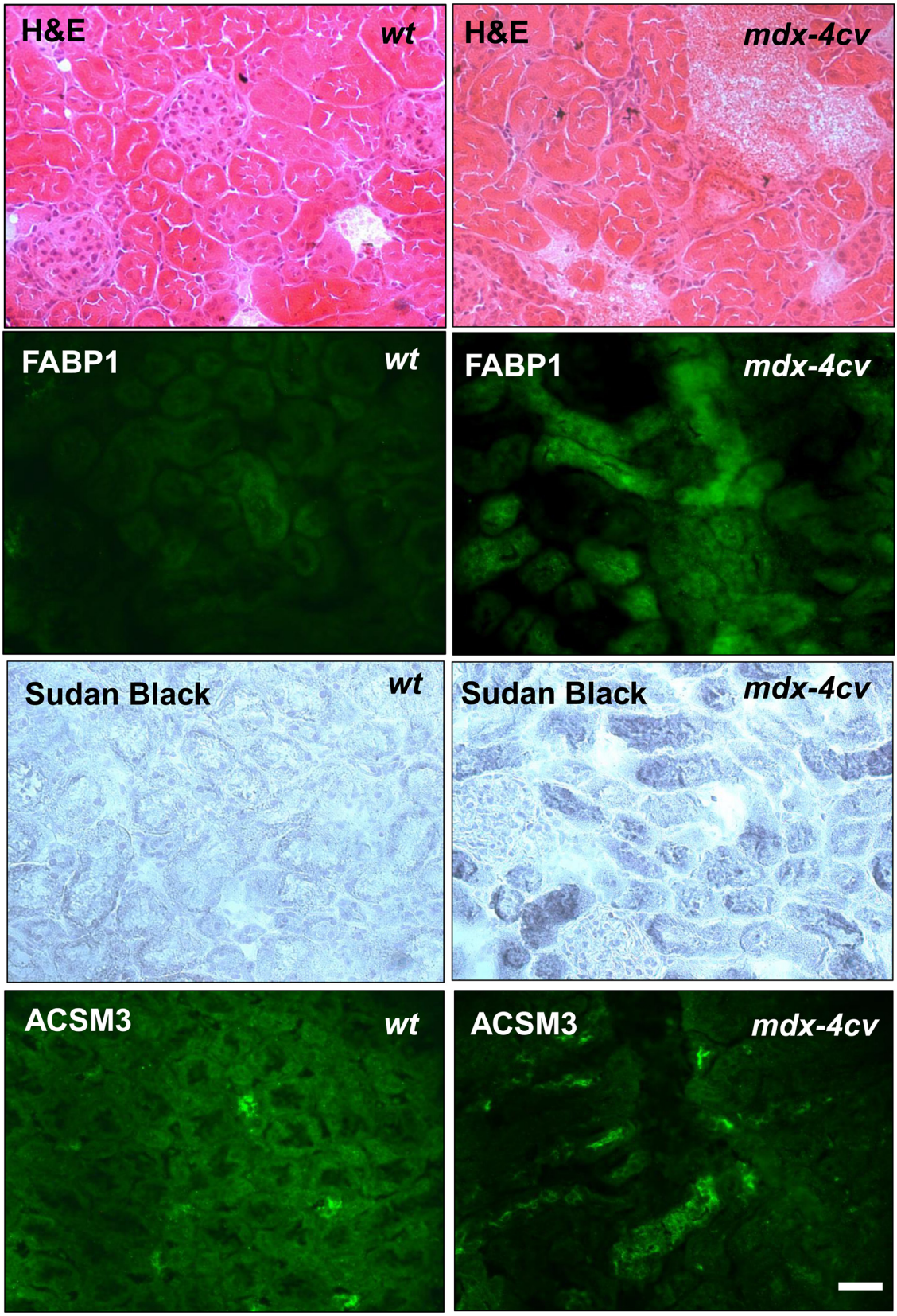


**Fig. 7.** Histological and immunofluorescence microscopical analysis of the *mdx-4cv* kidney. Shown are transverse sections of wild type (*wt*) versus *mdx-4cv* kidney stained with haematoxylin and eosin (H&E) or Sudan Black, as well as immuno-labelled with antibodies to fatty acid binding protein FABP1 or the ACSM3 isoform of mitochondrial acyl-coenzyme A synthetase. Bar equals 50 μm.

2019). The international effort to characterize the kidney proteome and the initiation of the Kidney and Urine Proteome Project (HKUPP) has led to the identification and cataloguing of several thousand kidney-associated protein species and dynamic proteo-forms in health and disease (Arthur et al., 2018; Cañadas-Garre et al., 2019; Klein and Schanstra, 2018). Transcriptomics in combination with antibody-based profiling of the human kidney has led to the establishment of the renal-specific protein complement including the identification of protein markers of distinct cellular structures, such as the glomeruli, proximal tubules, distal tubules and collecting ducts (Habuka et al., 2014). Building on these extensive proteomic maps of the kidney, this report has employed an Orbitrap Fusion Tribrid mass spectrometer for the comparative profiling of kidney preparations.

Proteome-wide changes appear to affect especially mitochondrial metabolism, the regulation of $Ca^{2+}$-homeostasis and the integrity of the extracellular matrix and focal adhesion complex in the *mdx-4cv* kidney. This makes the ACSM3 isoform of mitochondrial acyl-coenzyme A synthetase, as well as collagen COL-I, collagen COL-VI, prolargin and related basement membrane proteins, new biomarker candidates of renal changes in the *mdx-4cv* animal model. One of the most interesting pathobiochemical findings from the systematic proteomic analysis of the *mdx-4cv* kidney is the significant increase in the FABP1 isoform of fatty acid binding protein. FABP1 belongs to the protein family of intracellular lipid-binding proteins, which act as mediators of reversible binding of hydrophobic ligands and their subsequent trafficking through major subcellular systems (Thumser et al., 2014). The established FABP isoforms 1–9 have been named after their original discovery and abundance in particular tissues, such as L-FABP (liver), I-FABP (intestine), H-FABP (heart), A-FABP (adipocytes), E-FABP (epidermal tissue), Il-FABP (ileum), B-FABP (brain), M-FABP (myelin) and T-FABP (testis). The mass spectrometrically identified isoform FABP1 is also known as heme-binding protein, Z protein or hepatic FABP, and has been located in liver, kidney, intestine, pancreas, lung and stomach (Smathers and Petersen, 2011). Although the proteomic results and cell biological findings presented in this report do not demonstrate a direct functional link between increased FABP1 and fat accumulation, the findings indicate that the up-regulation of FABP1 may be related to abnormal fat metabolism. The elevated concentration of FABP1 might occur in association with ectopic fat deposition in the affected kidney, and this may play a pathophysiological role in renal dysfunction (Xu et al., 2015). The accumulation of ectopic fat might trigger impaired kidney performance, which may progress to the cardio-renal syndrome in dystrophinopathy (Villa et al., 2016).

Proteomic changes in fatty acid binding proteins suggest alterations in the binding of long-chain fatty acids and other lipophilic ligands (Thumser et al., 2014). Since fatty acid binding proteins also act as myokines and adipokines and function as regulators of metabolic signalling events, their altered concentration may be related to changes in metabolic control and associated cellular mechanisms (Hotamisligil and Bernlohr, 2015). The increased presence of FABP1 in the *mdx-4cv* kidney is reflected by its identification, together with FABP3 and FABP5, in the albumin-depleted serum from the *mdx-4cv* mouse (Murphy et al., 2017). Interestingly, FABP1 has recently been suggested as a general marker of chronic kidney damage (Lipiec et al., 2018). In addition, the increase of FABP1 in the *mdx-4cv* kidney is mirrored by a drastic up-regulation of FABP5 in the *mdx-4cv* liver, as determined by a proteomic survey of hepatic tissue (Murphy et al., 2018b). Thus, alterations in FABP1 and FABP5 can be useful as general pathobiochmical markers of secondary changes in kidney and liver tissue, respectively, in the *mdx-4cv* mouse model of dystrophinopathy.

In conclusion, the proteomic survey of the *mdx-4cv* kidney has shown a considerable increase in FABP1, which is probably related to abnormal fat deposits and disturbed fat metabolism. This makes this particular isoform of fatty acid binding protein an interesting new biomarker candidate for the evaluation of renal dysfunction in animal models of X-linked muscular dystrophy.

## Acknowledgements

Research was supported by Medical Research Charities Group grant HRB/MRCG-2016-20 from the Health Research Board and Muscular Dystrophy Ireland, as well as funding from the Kathleen Lonsdale Institute for Human Health Research at Maynooth University. The Orbitrap Fusion Tribrid mass spectrometer was funded under a Science Foundation Ireland Infrastructure Award to Dublin City University (SFI 16/RI/3701).

## References

Allen, D.G., Whitehead, N.P., Froehner, S.C., 2016. Absence of dystrophin disrupts skeletal muscle signaling: roles of $Ca^{2+}$, reactive oxygen species, and nitric oxide in the development of muscular dystrophy. Physiol. Rev. 96, 253–305.
Arthur, J.M., Karakala, N., Edmondson, R.D., 2018. Proteomic analysis for identification of biomarkers that predict severe acute kidney injury. Nephron 140, 129–133.
Askeland, E.J., Arlen, A.M., Erickson, B.A., Mathews, K.D., Cooper, C.S., 2013. Urological manifestations of Duchenne muscular dystrophy. J. Urol. 190, 1523–1528.
Bertrand, L.A., Askeland, E.J., Mathews, K.D., Erickson, B.A., Cooper, C.S., 2016. Prevalence and bother of patient-reported lower urinary tract symptoms in the muscular dystrophies. J. Pediatr. Urol. 12 (398) e1-398.e4.
Banks, G.B., Combs, A.C., Chamberlain, J.S., 2010. Sequencing protocols to genotype mdx, mdx(4cv), and mdx(5cv) mice. Muscle Nerve 42, 268–270.
Bladen, C.L., Salgado, D., Monges, S., Foncuberta, M.E., Kekou, K., Kosma, K., Dawkins, H., Lamont, L., Roy, A.J., Chamova, T., Guergueltcheva, V., Chan, S., Korngut, L., Campbell, C., Dai, Y., Wang, J., Barišić, N., Brabec, P., Lahdetie, J., Walter, M.C., Schreiber-Katz, O., Karcagi, V., Garami, M., Viswanathan, V., Bayat, F., Buccella, F., Kimura, E., Koeks, Z., van den Bergen, J.C., Rodrigues, M., Roxburgh, R., Lusakowska, A., Kostera-Pruszczyk, A., Zimowski, J., Santos, R., Neagu, E., Artemieva, S., Rasic, V.M., Vojinovic, D., Posada, M., Bloetzer, C., Jeannet, P.Y., Joncourt, F., Díaz-Manera, J., Gallardo, E., Karaduman, A.A., Topaloğlu, H., El Sherif, R., Stringer, A., Shatillo, A.V., Martin, A.S., Peay, H.L., Bellgard, M.I., Kirschner, J., Flanigan, K.M., Straub, V., Bushby, K., Verschuuren, J., Aartsma-Rus, A., Béroud, C., Lochmüller, H., 2015. The TREAT-NMD DMD Global Database: analysis of more than 7,000 Duchenne muscular dystrophy mutations. Hum. Mutat. 36, 395–402.
Braat, E., Hoste, L., De Waele, L., Gheysens, O., Vermeersch, P., Goffin, K., Pottel, H., Goemans, N., Levtchenko, E., 2015. Renal function in children and adolescents with Duchenne muscular dystrophy. Neuromuscul. Disord. 25, 381–387.
Bradford, M.M., 1976. A rapid and sensitive method for the quantitation of microgram quantities of protein utilizing the principle of protein-dye binding. Anal. Biochem. 72, 248–254.
Burch, P.M., Pogoryelova, O., Goldstein, R., Bennett, D., Guglieri, M., Straub, V., Bushby, K., Lochmüller, H., Morris, C., 2015. Muscle-derived proteins as serum biomarkers for monitoring disease progression in three forms of muscular dystrophy. J. Neuromuscul. Dis. 2, 241–255.
Cañadas-Garre, M., Anderson, K., McGoldrick, J., Maxwell, A.P., McKnight, A.J., 2019. Proteomic and metabolomic approaches in the search for biomarkers in chronic kidney disease. J. Proteomics 193, 93–122.
Carr, S.J., Zahedi, R.P., Lochmüller, H., Roos, A., 2018. Mass spectrometry-based protein analysis to unravel the tissue pathophysiology in Duchenne muscular dystrophy. Proteomics Clin. Appl. 12 (2). https://doi.org/10.1002/prca.201700071.
Chapman, V.M., Miller, D.R., Armstrong, D., Caskey, C.T., 1989. Recovery of induced mutations for X chromosome-linked muscular dystrophy in mice. Proc. Natl. Acad. Sci. U. S. A. 86, 1292–1296.
Cordova, G., Negroni, E., Cabello-Verrugio, C., Mouly, V., Trollet, C., 2018. Combined therapies for duchenne muscular dystrophy to optimize treatment efficacy. Front. Genet. 9, 114.
Danko, I., Chapman, V., Wolff, J.A., 1992. The frequency of revertants in mdx mouse genetic models for Duchenne muscular dystrophy. Pediatr. Res. 32, 128–131.
Delalande, O., Czogalla, A., Hubert, J.F., Sikorski, A., Le Rumeur, E., 2017. Dystrophin and Spectrin, two highly dissimilar sisters of the same family. Subcell. Biochem. 82, 373–403.
Dowling, J.J., Gonorazky, H.D., Cohn, R.D., Campbell, C., 2018. Treating pediatric neuromuscular disorders: the future is now. Am. J. Med. Genet. A 176, 804–841.
Dowling, P., Murphy, S., Zweyer, M., Raucamp, M., Swandulla, D., Ohlendieck, K., 2019. Emerging proteomic biomarkers of X-linked muscular dystrophy. Expert Rev. Mol. Diagn. 19, 739–755.
Ervasti, J.M., Ohlendieck, K., Kahl, S.D., Gaver, M.G., Campbell, K.P., 1990. Deficiency of a glycoprotein component of the dystrophin complex in dystrophic muscle. Nature 345, 315–319.
Fenton, R.A., 2018. Proteomic approaches in kidney disease biomarker discovery. Am. J. Physiol. Renal Physiol. 315, F1817–F1821.
Garimella, P.S., Sarnak, M.J., 2017. Uromodulin in kidney health and disease. Curr. Opin. Nephrol. Hypertens. 26, 136–142.
Goemans, N., Buyse, G., 2014. Current treatment and management of dystrophinopathies. Curr. Treat. Options Neurol. 16, 287.
Guiraud, S., Aartsma-Rus, A., Vieira, N.M., Davies, K.E., van Ommen, G.J., Kunkel, L.M., 2015. The pathogenesis and therapy of muscular dystrophies. Annu. Rev. Genomics Hum. Genet. 16, 281–308.
Gusel'nikova, V., Antimonova, O., Fedorova, E., Shavlovsky, M., Krutikov, A., Mikhailova, E., Gudkova, A., Mikhailov, V., Korzhevskii, D., 2018. Fluorescent characterization of

amyloid deposits in the kidneys of mdx mice. Eur. J. Histochem. 62, 2870.
Habuka, M., Fagerberg, L., Hallström, B.M., Kampf, C., Edlund, K., Sivertsson, Å., Yamamoto, T., Pontén, F., Uhlén, M., Odeberg, J., 2014. The kidney transcriptome and proteome defined by transcriptomics and antibody-based profiling. PLoS One 9, e116125.
Hathout, Y., Seol, H., Han, M.H., Zhang, A., Brown, K.J., Hoffman, E.P., 2016. Clinical utility of serum biomarkers in Duchenne muscular dystrophy. Clin. Proteomics 13, 9.
Holland, A., Dowling, P., Meleady, P., Henry, M., Zweyer, M., Mundegar, R.R., Swandulla, D., Ohlendieck, K., 2015. Label-free mass spectrometric analysis of the mdx-4cv diaphragm identifies the matricellular protein periostin as a potential factor involved in dystrophinopathy-related fibrosis. Proteomics 15, 2318–2331.
Holland, A., Murphy, S., Dowling, P., Ohlendieck, K., 2016. Pathoproteomic profiling of the skeletal muscle matrisome in dystrophinopathy associated myofibrosis. Proteomics 16, 345–366.
Hor, K.N., Mah, M.L., Johnston, P., Cripe, T.P., Cripe, L.H., 2018. Advances in the diagnosis and management of cardiomyopathy in Duchenne muscular dystrophy. Neuromuscul. Disord. 28, 711–716.
Hotamisligil, G.S., Bernlohr, D.A., 2015. Metabolic functions of FABPs–mechanisms and therapeutic implications. Nat. Rev. Endocrinol. 11, 592–605.
Im, W.B., Phelps, S.F., Copen, E.H., Adams, E.G., Slightom, J.L., Chamberlain, J.S., 1996. Differential expression of dystrophin isoforms in strains of mdx mice with different mutations. Hum. Mol. Genet. 5, 1149–1153.
Klein, J., Schanstra, J.P., 2018. Implementation of proteomics biomarkers in nephrology: from animal models to human application? Proteomics Clin. Appl. 2018, e1800089.
Koenig, M., Hoffman, E.P., Bertelson, C.J., Monaco, A.P., Feener, C., Kunkel, L.M., 1987. Complete cloning of the Duchenne muscular dystrophy (DMD) cDNA and preliminary genomic organization of the DMD gene in normal and affected individuals. Cell 50, 509–517.
Koenig, M., Monaco, A.P., Kunkel, L.M., 1988. The complete sequence of dystrophin predicts a rod-shaped cytoskeletal protein. Cell 53, 219–228.
Latimer, R., Street, N., Conway, K.C., James, K., Cunniff, C., Oleszek, J., Fox, D., Ciafaloni, E., Westfield, C., Paramsothy, P., Muscular Dystrophy Surveillance, Tracking, and Research Network (MD STAR net), 2017. Secondary Conditions among Males with Duchenne or Becker Muscular Dystrophy. J. Child Neurol. 32, 663–670.
Lindsay, A., Chamberlain, C.M., Witthuhn, B.A., Lowe, D.A., Ervasti, J.M., 2019. Dystrophinopathy associated dysfunction of Krebs cycle metabolism. Hum. Mol. Genet. 28, 942–951.
Lipiec, K., Adamczyk, P., Świętochowska, E., Ziora, K., Szczepańska, M., 2018. L-FABP and IL-6 as markers of chronic kidney damage in children after hemolytic uremic syndrome. Adv. Clin. Exp. Med. 27, 955–962.
LoMauro, A., D'Angelo, M.G., Aliverti, A., 2015. Assessment and management of respiratory function in patients with Duchenne muscular dystrophy: current and emerging options. Ther. Clin. Risk Manag. 11, 1475–1488.
Matsumura, T., Saito, T., Fujimura, H., Sakoda, S., 2012. Renal dysfunction is a frequent complication in patients with advanced stage of Duchenne muscular dystrophy. Rinsho Shinkeigaku 52, 211–217.
McGreevy, J.W., Hakim, C.H., McIntosh, M.A., Duan, D., 2015. Animal models of Duchenne muscular dystrophy: from basic mechanisms to gene therapy. Dis. Model. Mech. 8, 195–213.
Messina, S., Vita, G.L., 2018. Clinical management of Duchenne muscular dystrophy: the state of the art. Neurol. Sci. 39, 1837–1845.
Mi, H., Huang, X., Muruganujan, A., Tang, H., Mills, C., Kang, D., Thomas, P.D., 2017. PANTHER version 11: expanded annotation data from gene ontology and reactome pathways, and data analysis tool enhancements. Nucleic Acids Res. 45, D183–D189.
Momper, J.D., Nigam, S.K., 2018. Developmental regulation of kidney and liver solute carrier and ATP-binding cassette drug transporters and drug metabolizing enzymes: the role of remote organ communication. Expert Opin. Drug Metab. Toxicol. 14, 561–570.
Moriuchi, T., Fujii, Y., Kagawa, N., Hizawa, K., 1991. Autopsy study on the weight of the heart, liver, kidney and brain in Duchenne muscular dystrophy. Tokushima J. Exp. Med. 38, 5–13.
Motoki, T., Shimizu-Motohashi, Y., Komaki, H., Mori-Yoshimura, M., Oya, Y., Takeshita, E., Ishiyama, A., Saito, T., Nakagawa, E., Sugai, K., Murata, M., Sasaki, M., 2015. Treatable renal failure found in non-ambulatory Duchenne muscular dystrophy patients. Neuromuscul. Disord. 25, 754–757.
Muntoni, F., Torelli, S., Ferlini, A., 2003. Dystrophin and mutations: one gene, several proteins, multiple phenotypes. Lancet Neurol. 2, 731–740.
Murphy, S., Ohlendieck, K., 2015. The biochemical and mass spectrometric profiling of the dystrophin complexome from skeletal muscle. Comput. Struct. Biotechnol. J. 14, 20–27.
Murphy, S., Dowling, P., Zweyer, M., Henry, M., Meleady, P., Mundegar, R.R., Swandulla, D., Ohlendieck, K., 2017. Proteomic profiling of mdx-4cv serum reveals highly elevated levels of the inflammation-induced plasma marker haptoglobin in muscular dystrophy. Int. J. Mol. Med. 39, 1357–1370.
Murphy, S., Zweyer, M., Mundegar, R.R., Swandulla, D., Ohlendieck, K., 2018a. Comparative gel-based proteomic analysis of chemically crosslinked complexes in dystrophic skeletal muscle. Electrophoresis 39, 1735–1744.
Murphy, S., Zweyer, M., Henry, M., Meleady, P., Mundegar, R.R., Swandulla, D., Ohlendieck, K., 2018b. Proteomic profiling of liver tissue from the mdx-4cv mouse model of Duchenne muscular dystrophy. Clin. Proteomics 15, 34.
Murphy, S., Zweyer, M., Henry, M., Meleady, P., Mundegar, R.R., Swandulla, D., Ohlendieck, K., 2019a. Proteomic analysis of the sarcolemma-enriched fraction from dystrophic mdx-4cv skeletal muscle. J. Proteomics 191, 212–227.
Murphy, S., Zweyer, M., Raucamp, M., Henry, M., Meleady, P., Swandulla, D., Ohlendieck, K., 2019b. Proteomic profiling of the mouse diaphragm and refined mass spectrometric analysis of the dystrophic phenotype. J. Muscle Res. Cell. Motil. 40, 9–28.
Ohlendieck, K., Matsumura, K., Ionasescu, V.V., Towbin, J.A., Bosch, E.P., Weinstein, S.L., Sernett, S.W., Campbell, K.P., 1993. Duchenne muscular dystrophy: deficiency of dystrophin-associated proteins in the sarcolemma. Neurology 43, 795–800.
Partridge, T.A., 2013. The mdx mouse model as a surrogate for Duchenne muscular dystrophy. FEBS J. 280, 4177–4186.
Reay, D.P., Bastacky, S.I., Wack, K.E., Stolz, D.B., Robbins, P.D., Clemens, P.R., 2015. D-amino acid substitution of peptide-mediated NF-κB suppression in mdx mice preserves therapeutic benefit in skeletal muscle, but causes kidney toxicity. Mol. Med. 21, 442–452.
Rodrigues, M., Echigoya, Y., Fukada, S.I., Yokota, T., 2016. Current translational research and murine models for duchenne muscular dystrophy. J. Neuromuscul. Dis. 3, 29–48.
Rysz, J., Gluba-Brzózka, A., Franczyk, B., Jabłonowski, Z., Ciałkowska-Rysz, A., 2017. Novel biomarkers in the diagnosis of chronic kidney disease and the prediction of its outcome. Int. J. Mol. Sci. 18 pii: E1702.
Shin, J.H., Hakim, C.H., Zhang, K., Duan, D., 2011. Genotyping mdx, mdx3cv, and mdx4cv mice by primer competition polymerase chain reaction. Muscle Nerve 43, 283–286.
Shumyatcher, Y., Shah, T.A., Noritz, G.H., Brouhard, B.H., Spirnak, J.P., Birnkrant, D.J., 2008. Symptomatic nephrolithiasis in prolonged survivors of Duchenne muscular dystrophy. Neuromuscul. Disord. 18, 561–564.
Singh, M., Jacobs, I.B., Spirnak, J.P., 2007. Nephrolithiasis in patients with duchenne muscular dystrophy. Urology 70, 643–645.
Smathers, R.L., Petersen, D.R., 2011. The human fatty acid-binding protein family: evolutionary divergences and functions. Hum. Genomics 5, 170–191.
Spitali, P., Hettne, K., Tsonaka, R., Charrout, M., van den Bergen, J., Koeks, Z., Kan, H.E., Hooijmans, M.T., Roos, A., Straub, V., Muntoni, F., Al-Khalili-Szigyarto, C., Koel-Simmelink, M.J.A., Teunissen, C.E., Lochmüller, H., Niks, E.H., Aartsma-Rus, A., 2018. Tracking disease progression non-invasively in Duchenne and Becker muscular dystrophies. J. Cachexia Sarcopenia Muscle 9, 715–726.
Szklarczyk, D., Morris, J.H., Cook, H., Kuhn, M., Wyder, S., Simonovic, M., Santos, A., Doncheva, N.T., Roth, A., Bork, P., Jensen, L.J., von Mering, C., 2017. The STRING database in 2017: quality-controlled protein-protein association networks, made broadly accessible. Nucleic Acids Res. 45, D362–D368.
Thumser, A.E., Moore, J.B., Plant, N.J., 2014. Fatty acid binding proteins: tissue-specific functions in health and disease. Curr. Opin. Clin. Nutr. Metab. Care 17, 124–129.
Tichy, E.D., Mourkioti, F., 2017. A new method of genotyping MDX4CV mice by PCR-RFLP analysis. Muscle Nerve 56, 522–524.
Tidball, J.G., Welc, S.S., Wehling-Henricks, M., 2018. Immunobiology of inherited muscular dystrophies. Compr. Physiol. 8, 1313–1356.
Villa, C.R., Kaddourah, A., Mathew, J., Ryan, T.D., Wong, B.L., Goldstein, S.L., Jefferies, J.L., 2016. Identifying evidence of cardio-renal syndrome in patients with Duchenne muscular dystrophy using cystatin C. Neuromuscul. Disord. 26, 637–642.
Viollet, L., Gailey, S., Thornton, D.J., Friedman, N.R., Flanigan, K.M., Mahan, J.D., Mendell, J.R., 2009. Utility of cystatin C to monitor renal function in Duchenne muscular dystrophy. Muscle Nerve 40, 438–442.
Wada, E., Hamano, T., Matsui, I., Yoshida, M., Hayashi, Y.K., Matsuda, R., 2019. Renal involvement in the pathogenesis of mineral and bone disorder in dystrophin-deficient mdx mouse. J. Physiol. Sci. 69, 661–671.
Wilson, K., Faelan, C., Patterson-Kane, J.C., Rudmann, D.G., Moore, S.A., Frank, D., Charleston, J., Tinsley, J., Young, G.D., Milici, A.J., 2017. Duchenne and Becker muscular dystrophies: a review of animal models, clinical end points, and biomarker quantification. Toxicol. Pathol. 45, 961–976.
Wiśniewski, J.R., Zougman, A., Mann, M., 2009. Combination of FASP and StageTip-based fractionation allows in-depth analysis of the hippocampal membrane proteome. J. Proteome Res. 8, 5674–5678.
Xie, J.X., Li, X., Xie, Z., 2013. Regulation of renal function and structure by the signaling Na/K-ATPase. IUBMB Life 65, 991–998.
Xu, Y., Xie, Y., Shao, X., Ni, Z., Mou, S., 2015. L-FABP: a novel biomarker of kidney disease. Clin. Chim. Acta 445, 85–90.
Zhang, A., Uaesoontrachoon, K., Shaughnessy, C., Das, J.R., Rayavarapu, S., Brown, K.J., Ray, P.E., Nagaraju, K., van den Anker, J.N., Hoffman, E.P., Hathout, Y., 2015. The use of urinary and kidney SILAM proteomics to monitor kidney response to high dose morpholino oligonucleotides in the mdx mouse. Toxicol. Rep. 2, 838–849.
Zhang, W.R., Parikh, C.R., 2019. Biomarkers of acute and chronic kidney disease. Annu. Rev. Physiol. 81, 309–333.